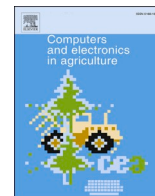




Contents lists available at ScienceDirect

Computers and Electronics in Agriculture

journal homepage: www.elsevier.com/locate/compag

Original papers

Computer vision-based citrus tree detection in a cultivated environment using UAV imagery

Cenk Donmez^{a,b,*}, Osman Villi^c, Suha Berberoglu^a, Ahmet Cilek^a^a Cukurova University, Landscape Architecture Department, Remote Sensing and GIS Lab, 01330 Adana, Turkey^b Leibniz Centre for Agricultural Landscape Research (ZALF), Eberswalder Str. 84, 15374 Muencheberg, Germany^c Toros University, Computer Technologies Department, Mersin, Turkey

ARTICLE INFO

Keywords:

Unmanned air vehicles
Morphological image operations
Precision agriculture
Tree detection
Computer vision

ABSTRACT

Manual inspection has been a common application for counting the trees and plants in orchards in precision agriculture processes. However, it is a time-consuming and, labour-intensive and expensive task. Recent remote sensing tools and methods provide a revolutionizing innovation for monitoring individual trees and crop recognition as an alternative to manual detection useful for long-term agricultural management. Our study adopted a Connected Components Labeling (CCL) algorithm to detect and count the citrus trees based on the high-resolution Unmanned Air Vehicles (UAV) images in two agricultural patches. The workflow consisted of applying morphological image operation algorithms on multi-spectral, 5-banded orthophoto imagery (derived from 1560 scenes) and 3,57 cm spatial resolution. Our approach was able to count 1462 out of 1506 trees resulting in accuracy and precision higher than 95% (*average Recall: 0.97, Precision: 0.95*) in heterogeneous agricultural patches (multiple trees and tree sizes). According to our understanding, the first time a CCL algorithm has been used with UAV multi-spectral images for detecting citrus trees. It performed significantly for geolocation and counting the trees individually in a heterogenous orchard. We concluded that our methodology provided satisfactory performance to predict the number of trees (in the citrus case study) in dense patches. Therefore it could be promising to replace the conventional tree detection techniques to detect the orchard trees in complex agricultural regions.

1. Introduction

Remote sensing is an essential component for precision agriculture, which has a significant role in agricultural sustainability (Hunt and Daughtry, 2018). It has been used commonly in percent tree cover (Donmez et al., 2015), land use/land cover mapping (Aplin, 2004; Thyagarajan and Vignesh, 2019), forest fire mapping (Satir et al., 2016), soil management (Cilek et al., 2020), plant diseases and detection (Zhang et al., 2019; Lin et al., 2019; Thyagarajan and Kiruba Raji, 2019), etc. Developing sophisticated methods for detecting and counting orchard trees from high-resolution imagery is one of its recent research efforts and focuses on efficient agricultural management and productivity. Incorporating optical imagery and ground data can provide significant assets to improve agricultural production and to monitor vegetation and tree health in their growing (Torres-Sánchez et al.,

2015).

Detecting and counting the trees in an orchard is necessary for yield prediction/monitoring and pest management in particular. In developing countries such as Turkey, manual sampling methods, which physically record the trees by Ground Positioning System (GPS), are commonly used in tree counting and agricultural monitoring processes. These methods are expensive, labour-intensive, slow, and time-consuming to update for continuous monitoring. In recent years, there was a high concern about the use of UAVs in many industries, including agricultural applications (Belgiu and Csillik, 2018; Torres-Sánchez et al., 2015). A common concern has been noticed on the literature surveys on increasing UAV usage, especially in precision agriculture. For instance, high-resolution data provided by UAV-mounted sensors often paired with different sensors assist farmers in the field management in precision agriculture (Csillik et al., 2018; Deng et al., 2018; Hunt and

* Corresponding author at: Cukurova University, Department of Landscape Architecture, Remote Sensing and GIS Lab., 01330 Adana, Turkey and Leibniz-Centre for Agricultural Landscape Research (ZALF), Eberswalder Str. 84, 15374, Muencheberg, Germany.

E-mail addresses: cdonmez@cu.edu.tr, Cenk.Doenmez@zalf.de (C. Donmez), osman.villi@toros.edu.tr (O. Villi), suha@cu.edu.tr (S. Berberoglu), acilek@cu.edu.tr (A. Cilek).

<https://doi.org/10.1016/j.compag.2021.106273>

Received 21 February 2021; Received in revised form 7 June 2021; Accepted 11 June 2021

Available online 18 June 2021

0168-1699/© 2021 Elsevier B.V. All rights reserved.

Daughtry, 2018; Yang, 2020, 2012). They can mainly be advantageous to accelerate the tree detecting and counting process compared to conventional techniques. In orchard tree detection, the UAVs have an indisputable potential in various scales from small to large cultivated patches.

Many studies showed the UAVs' remarkable advantages for crop monitoring (e.g., corn and wheat, citrus) (Mattos et al., 2018). They provide low-cost image acquisition methods for using in tree detection analysis, mainly in agricultural applications (Csillik et al., 2018; Hall et al., 2018; Hentschke et al., 2018). For instance, palm trees were detected by Malek et al. (2014) using a learning machine classifier. Position and heights of the orchard trees were estimated using point clouds and orthophoto derived from multi-spectral UAV imagery by Surovy et al. (2018) by combining Hough transformation and morphological image operations (Al Mansoori et al., 2018). Similarly, Deep Learning (DL) algorithms have also been applied in UAV-based remote sensing applications (Ampatzidis and Partel, 2019; Csillik et al., 2018; Díaz-Varela et al., 2015; Jiang et al., 2017). In general, DL algorithms comprise unsupervised and supervised feature-learning as well as neural network algorithms. Among these, Convolutional Neural Network (CNN) showed a remarkable performance in agricultural fields and studies, including tree counting (Chen et al., 2017), crop density estimation (Madec et al., 2019), and object (Vazquez-Nicolas et al., 2020) and plant detection (Djerriri et al., 2018).

Sophisticated methods to monitor orchard trees are needed for better agricultural and crop management. Using automated methods and algorithms in a comprehensive approach can be an effective alternative to manual delineation and counting trees for long-term future crop rotations. For counting and detecting the trees, various techniques have been applied and adapted to UAV imagery (Osco et al., 2020). Orchard trees, including citrus plantations, have been delineated using automatized approaches in agricultural patches (Ozdarici-Ok, 2015). CNN method was implemented in multi-spectral UAV images with a precise and reasonable agreement (Ampatzidis and Partel, 2019; Csillik et al., 2018). It has a hierarchical architecture that can be trained to perform object recognition and detection.

Besides object-based classification, pixel-based classification algorithms were also used for object detection, such as k-means (Celik, 2009), neural networks (Miller et al., 1995), and support vector machines (Mountrakis et al., 2011). With the ever-growing available VHR remote-sensing images, conventional pixel-based classification approaches were sensitive in these studies. Detecting and counting objects are the effective pixel-based feature extraction methods commonly used in computer vision and image processing applications (Campos et al., 2017). The core task for object recognition from the UAV data is to provide relevant data sets for crop and orchard management. It represents the object recognition and extraction (i.e. trees) from the multi-spectral imagery with high resolution.

Connected-component labelling (CCL) algorithms provide effective solutions in component extraction and detection in image processing. CCL counts the various objects on an image, and it is one of the most fundamental operations in image processing. It is an effective computer vision algorithm based on the connected component techniques (4, 6, 8-connected) to detect linked regions in binary digital images. The image is scanned pixel by pixel sequentially, and a label to every foreground pixel in the binary image is assigned (Dharpure et al., 2013). Besides, high dimensional data and color images can also be processed using the CCL algorithms.

To remove the imperfections in a binary image, including noise, texture, and shapes, morphological image operations are used and usually engaged with CCL. The misclassified regions are eliminated using morphological operations by applying some spatial features to the clustered image (Ramesh et al., 2016). The connected components between the pixels can be detected by the CCL combined with the morphological operations in a binary image, including color or grayscale ranges, by proper thresholding (Acharya and Ray, 2005). Converted

high-dimensional color or greyscale images can also be processed. Many research has been published on automatic target detection using computer vision, including mathematical morphology, Gabor filters (Jain et al., 1997), and temporal-based methods such as maximum likelihood and dynamic programming (Diani et al., 2001).

Many studies have accurately detected and counted citrus trees using object-based techniques (e.g., CNN) in UAV multi-spectral images (Csillik et al., 2018; Ozdarici-Ok, 2015; Verma et al., 2016). Our methodology is based on a pixel-based CCL algorithm that detects each plant individually using rectangles. Considerably, the difficulty of discriminating individual plants may increase if the orchard is crowded and the plant size decreases. Therefore, the rectangle can not be detected if the geometry of individual plants may not be sufficiently visible. In this case, the CCL can operate on pixel information by integrating image recognition and completes labeling of the objects in a two-scan procedure (He et al., 2012) by assigning the label to each pixel based on its neighbours (connectivity). However, the performance of CCL to detect and count citrus trees in considering high-density agricultural patches is still unknown.

In our paper, we address the mentioned gap and present a CCL approach to cope with the challenge of detecting citrus trees in agricultural regions from UAV multi-spectral images. Our method not only provides the detecting but also counting of citrus trees in a patch. Regarding these issues, the study aims to adopt and implement a CCL approach for detecting and counting citrus trees in multi-spectral images acquired from a UAV sensor. A comprehensive computer vision technique was implemented based on combining morphological filtering and CCL on multi-spectral images in a two-scan procedure. Compared to conventional methods, combining computer vision and UAV data is extremely important for developing cutting-edge techniques to produce frequent, cost-effective, and accurate monitoring data for better agricultural management. In this point of view, our study aimed to reveal an innovative approach for efficient irrigation, fertilization, and crop management in agricultural regions. The proposed method and outputs of the paper are organized as follows: Section 2 provides information on the study area and materials used, including UAV implementation; Section 3 describes the proposed methodological steps in detail; Section 4 reflects the operational results; Section 5 reflects the discussion and conclusions of the study.

2. Study sites and materials

2.1. Study site

The study area is located at the experimental agricultural fields of Cukurova University, in Adana city in the Eastern Mediterranean part of Turkey (Fig. 1).

Turkey provides 2.75% of the world's total citrus production and growth potential associated with many fruits and vegetables due to its suitable climatic and ecological conditions. Citrus fields in Turkey cover 127.342 ha, and Cukurova is the leading agricultural region, which provides 77% of Turkey's citrus production. Three main citrus types, including orange (Navelina, Valencia, Washington-Navel), lemon, and mandarin (Okitsu, Nour, Nova, Minneola, Tangelo), are cultivated; however, there has been a remarkable decrease in citrus production in the region in recent years (NCA, 2020).

We have selected two agricultural parcels, covering 73.5 ha with Washington-Navel orange trees with six by 1.6 m spacing. These trees were almost six years old and about 3–4 m high, in mature and production stages. The civil aviation authorisation of Turkey was informed about the UAV operations in the study area.

2.2. Setting up the UAV equipment and multi-spectral camera

A multi-copter (V8 Octocopter) of DJI was used for image acquisition of the citrus parcels in the study area (Fig. 2). The equipment of the UAV

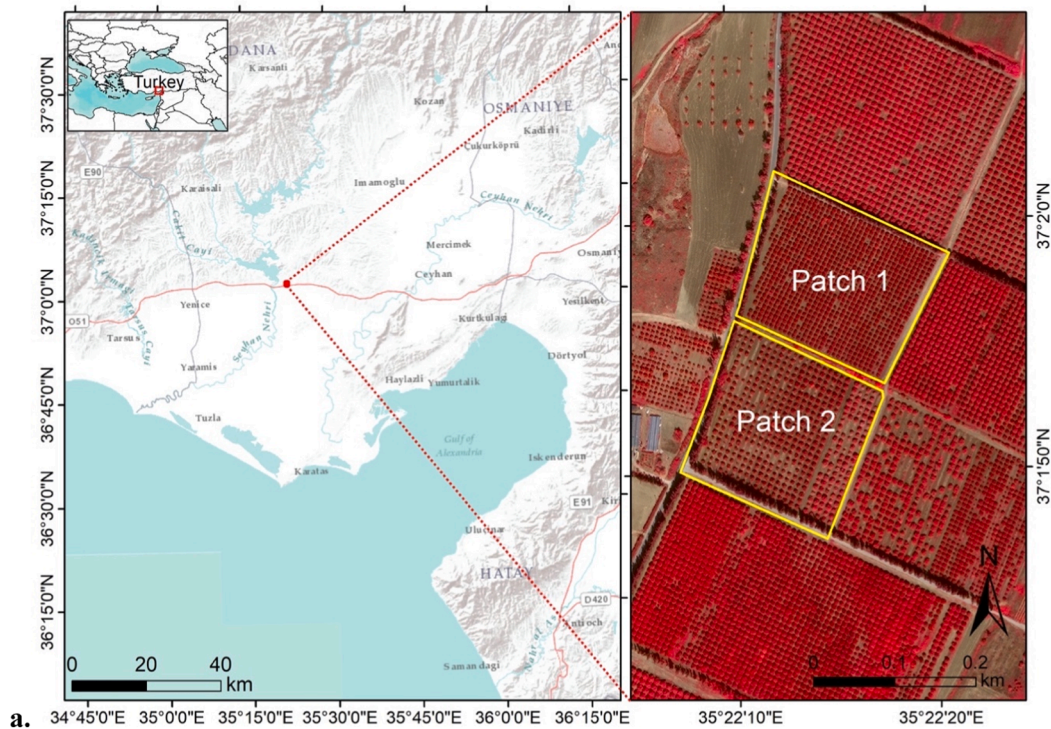


Fig. 1. Location of the study area (Adana, Turkey) (a) (left) and a false-color image acquired by the UAV (right). Citrus plantations at the study site (b1 and b2).



Fig. 2. DJI octocopter (V8) used for image acquisition in the study.

system was implemented and adapted in Cukurova University, Remote Sensing, and GIS Laboratory. The UAV equipment has a high load-carrying capacity, the ability to access and effective use in a small study site, and low flying altitudes.

For an optimal tracking accuracy of the multi-copter, three GPS receivers and antennas were integrated to work simultaneously. These receivers also have combined Inertial Measurement Unit (IMU) sensors to allow GPS for calculating metrics (attitude, angular rates, position, etc.) relative to a global reference frame in possible signal deficits. Using an IMU provides considerable advantages for the precision and reliability of the dynamic UAV applications at the lowest possible cost.

The UAVs get their energy to power their engines from either fuel or electricity. Fuel engine UAVs are primarily used in military and defense projects, while electric engine ones are more common and accessible for research purposes. The UAV used in our study included eight engines, and each engine had 150 to 170 RPM rev/min. These engines demanded high electricity capacity; thus, we integrated a rechargeable Li-Po (Lithium Polymer) battery to provide approximately 25 min of safe flight time. The battery consisted of 6-connected cells with 25.2 V (nominal voltage) and 22.000 mAH capacity, which could draw 2.2. ampere for 1 h. We have taken out the capacity of the battery in flight planning.

GPS and antenna positions were recorded through the A3 Pro flight controller onboard to perform image transfer and instant telemetry data from the UAV (Fig. 3a). The IMU sensor, engine detector, Electronic Speed Controller (ESC), engine directions, and controller settings have been configured and recorded on the A3 Pro manually (Fig. 3b). In

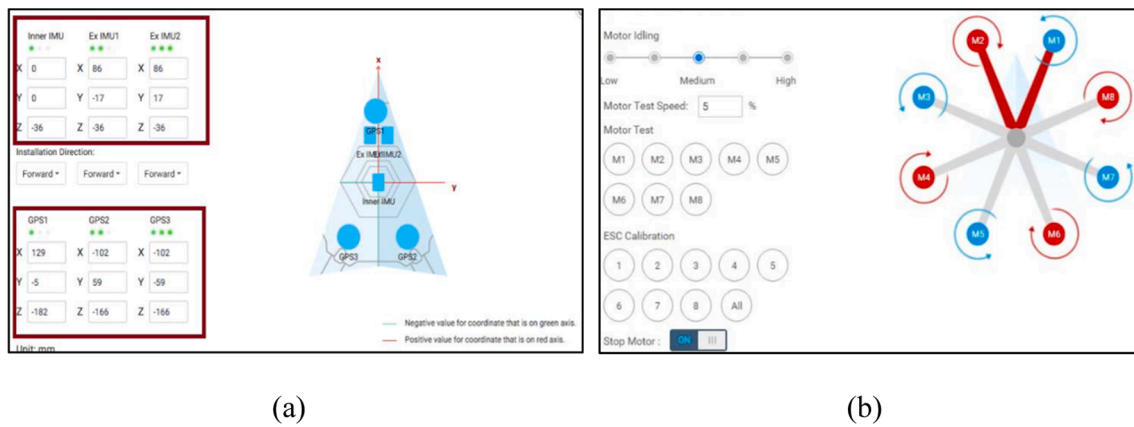


Fig. 3. GPS positions and IMU settings (a) and engine directions (b) of the UAV used in the study.

case of an unexpected situation during the flight (i.e., wind changes), operational safety settings (i.e., autonomous pilot control) were also configured.

Micasense Red edge 5-band sensor was used for image acquisition, designed primarily for small UAV systems. It provides multi-band data for precision agriculture applications, particularly for vegetation mapping with a 5-volt operating voltage, approx. 150 g weight and 8 cm pixel ground sampling (at 120 m flight altitude). Its bands capture Blue (centered on 475 nm), green (560 nm), red (668 nm), near-infrared (NIR, 840 nm), and Red edge (717 nm), allowing for accurate detection of vegetation health and discriminate species based on their spectral signatures (Micasense, 2015). Details of the camera are given in Table 1. A3 Pro, IMU systems, and a Multi-spectral camera used on the DJI V8 Octocopter are presented in Fig. 4.

2.3. UAV image acquisition

Image acquisition with the DJI V8 octocopter was carried out from 55 m altitude at 5 m/s speed in clear conditions between 13:30 – 14:30 to minimize the shadow effects on the images and alternating lighted and dark areas (Campos et al., 2016). The wind speed was between 2 and 3 m/s, and no precipitation occurred. The UAV and the multi-spectral camera were used with an average 80% overlap (along and across). The UAV was operated at a 23.2 m Mean Sea Level (MSL) and 55 m Above Ground Level (AGL) to maximize resolution and potential coverage area. Two flight operations were carried out and 1560 multi-spectral images were recorded (flight 1 = 899, flight 2 = 661). The planning and routing of Flight 1 are represented in Fig. 5.

2.4. Image processing

Digital Surface Model (DSM), orthophoto, and Normalized Difference Vegetation Index (NDVI) maps were derived from UAV imagery as main inputs for detecting and counting citrus trees separately in our methodology. The images were geometrically corrected and prepared to include in the CCL processes.

Point cloud

In the first step, point cloud data were derived and photogrammetrically processed for deriving DSM and orthophoto images using

Pix4D software (Pix4D, 2018). Image reference points were generated using point cloud and mesh techniques for mosaicing the obtained images from the UAV with high accuracy. Depending on the quality of the acquisition images and the terrain type, 907,011 points were derived (14 per/m³) in the point cloud using the default settings of the Pix4D algorithm. Following, tie-points of these images were generated on the overlapping images and used to derive DEM and orthophoto mosaics. Point cloud images are given in Fig. 6, and their processing options and densification details in Table 2.

Orthorectification and NDVI derivation

The orthorectification was performed after deriving the point cloud using Pix4DMapper. A dual-frequency GNSS (Global Navigation Satellite System) was utilized to survey nine ground control points (GCPs). Boundaries of the orchards were defined by determining GNSS baselines between the polygonal points of the study sites based on these GCPs. Acquired images were corrected radiometrically based on the reference plate's radiance values derived using the Micasense Red edge camera before the flight. More than two overlapping images were used to produce 5-band orthophoto mosaics with 3.7 cm spatial resolution. These images were georeferenced with WGS84, Zone 36 (UTM) projection. Examples of the Red, Green, Blue, Near-IR, Red Edge orthophotos are provided in Fig. 7. NDVI maps were derived using Near-IR and Red band combination from the orthophoto images (Eq. (1)).

A Digital Surface Model (DSM) is a topography associated image of the earth's surface representing natural or human-made features located on the ground. As one of the input layers, we produced the DSM to obtain reliable data about the object heights, therefore extracting the citrus trees with higher accuracy. The point cloud data derived from the UAV was used to compute a DSM in the Pix4D environment.

$$NDVI = \frac{(\text{NearIR} - \text{Red})}{(\text{NearIR} + \text{Red})} \quad (1)$$

In the DSM derivation process, a point cloud-based information was interpolated for the entire area. Missing cells in the point cloud were filled from the neighboring points. Then, a surface smoothing algorithm was applied to the generated DSM based on selecting the radius of the median filter. For keeping the surface orientation and thus, sharp features (i.e. tree regions), low smoothing values were appointed, and the DSM was delineated.

3. Method

A new and comprehensive delineation method for multi-spectral imagery was proposed in our study to improve orchard tree detection. The method is based on adapting the CCL process to high-resolution UAV imagery in a citrus tree case study. The workflow of the methodology, depicted in Fig. 8, includes four main steps; (i) grayscale operation and histogram equalization of the main inputs (DEM, 5-band

Table 1
Micasense Red edge camera details.

Bands	Bandwidth (nm)	Wavelength (nm)	Resolution
Green	20	560	Spatial (3.7 cm)
Red	10	668	HFOV 47 ⁰
Red edge	10	717	VFOV 37 ⁰
NIR	40	840	DFOV 58 ⁰

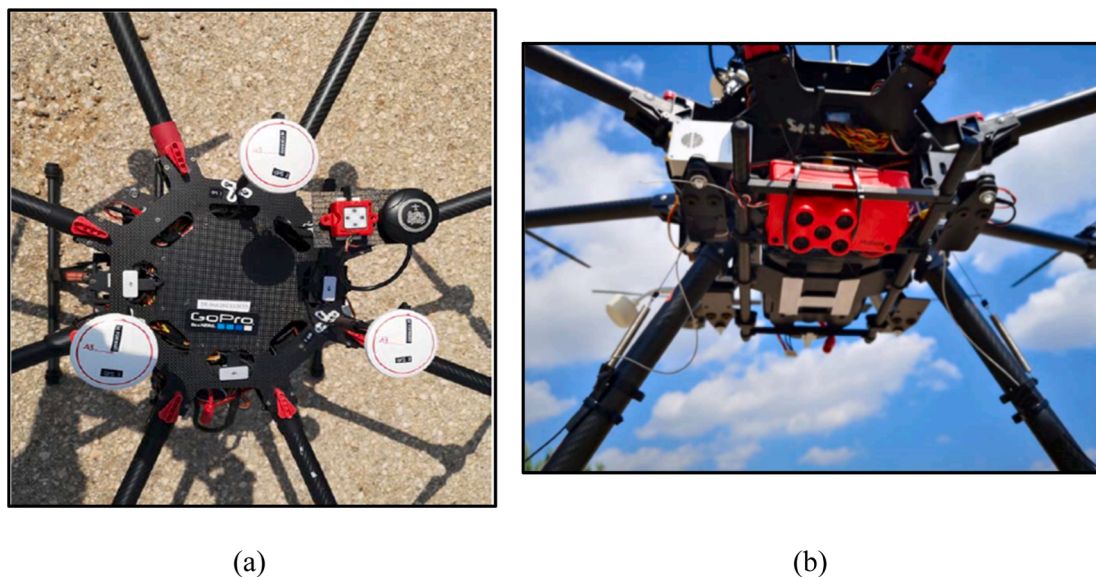


Fig. 4. A3 Pro and IMU systems (a) and mounted multi-spectral camera (b) on the DJI V8 Octocopter used in image acquisition for the study.

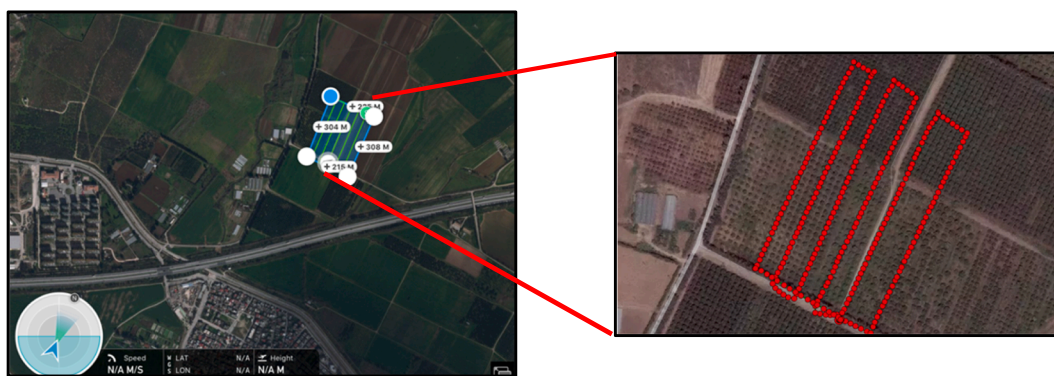


Fig. 5. Planning (left) and routing (right) of Flight 1 (red dots represent the acquired images). (For interpretation of the references to color in this figure legend, the reader is referred to the web version of this article.)

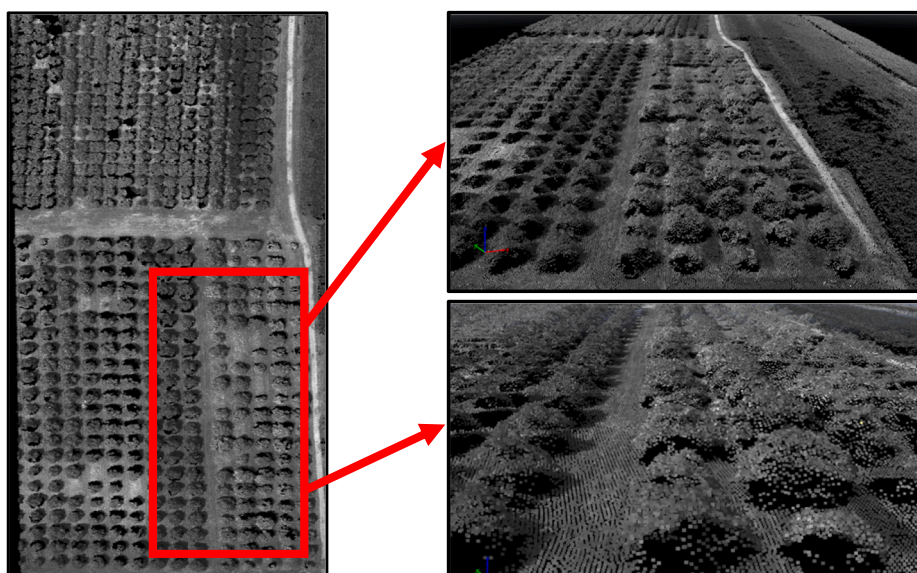


Fig. 6. Point cloud images of the study site (derived using 907,011 points).

Table 2

Point cloud processing options and densification details.

Processing options	Settings
Image scale	Multiscale, ½ (half image size, default)
Point density	Low
Minimum number of matches	3
3D textured Mesh Generation	Yes, Color balancing: No
Advanced: 3D Textured Mesh Settings	Sample Density Divider: 1
Image group	Blue, Green, Red, Near-IR, Red Edge
Time for Point Cloud Densification	02 min:11 s
Number of Generated Tiles	1
Number of 3D Densified Points	907,011
Average Density (per m ³)	14.8

orthophotos, NDVI) from the multi-spectral images, (ii) applying mathematical morphological image operations (opening and closing) for each band to obtain the gradient images, (iii) deriving binary formats, (iv) employing 8-connected CCL algorithm to the multi-spectral images in a two-scan way to obtain final citrus detection and count maps. The proposed approach was developed and implemented in the MATLAB environment.

3.1. Grayscale operations and histogram equalization

Grayscale image operations (also known as grayscale morphology) are used to extract image components (i.e., object shapes) by picking out small bright or dark features in an image. Indeed, gray color is one in which the RGB components all have equal intensity in the image. A single intensity value is necessary to specify for each pixel only for extracting the objects, as opposed to the tree intensities needed to identify each pixel in a full-color image. Thus, we used grayscale operations to differentiate the total amount of emitted light for each pixel of the multi-spectral images; to capture the dark and bright pixels. In the study, the grayscale images were derived in 16-bit as entirely sufficient assets to simplify tree detection and count processes contrary to using detailed color images, as follows where O_{ixj} is Multi-spectral Image G_{ixj} is a grayscale image (Eq. (2)).

$$G_{ixj} = (O_{ixj}^{Red} * 0.2989) + (O_{ixj}^{Green} * 0.5870) + (O_{ixj}^{Blue} * 0.1140) \quad (2)$$

After grayscale morphological operations, Histogram Equalization (HE) technique was applied for the contrast enhancements of the images. It stretches out the intensity range and increases the global contrast of the images with close contrast values. Therefore, HE was useful in our study to enhance the contrast since our multi-spectral UAV images consisted of a bright and dark background, which were complicated for tree detection.

HE cannot be applied separately to the RGB components of the image as it leads to dramatic changes in the color balance of an image set since, the RGB image representation is far from the human concept of color. Color features are highly related, and it is not possible to assess the similarity of two colors from their distance in this space in the multi-spectral RGB images (Golland and Bruckstein, 1996). Thus, we converted the images to the grayscale to apply the HE algorithm without changing the hue and saturation of the image (Eq. (3)). The contrast distribution of the acquired, grayscale images and HE are shown in Fig. 9.

$$S_k = \sum_{j=0}^k \left(\frac{n_j}{n} \right) (L-1)k = 0, 1, 2, 3, \dots, L-1. \quad (3)$$

where, n : total number of pixels in the input image ($n_0 + n_1 + \dots + n_{L-1} = n$), n_j (n_k): j . The number of the gray pixels, L : Desired number of the gray pixels, S_k : gray conversion threshold for the contrast enhancement. The grayscale values of pixels were altered to take advantage of the available shades of gray to become distributed across the full grayscale range.

The process of image grayscale is one of the main steps of image

processing. It enables the morphological processes to give more precise results on the image. For instance, histogram, morphological operations, filter applications, etc., could be implemented more efficiently than the color image due to converting the images to gray. In our study, the UAV images recorded in different bands have been converted to the grayscale to implement object detection and counting easier. Converting the images to the grayscale allowed us to apply HE and opening-closing morphological procedures for image enhancement.

3.2. Image morphological operations

Morphological processing was the next step after employing grayscale and histogram equalization operations using non-linear operations linked to the features (shape and morphology) in an image. The relative ordering of pixel values is mainly relied upon and suited to processing binary and grayscale images. A morphological image processing process includes many compound operations, commonly including dilation, erosion, opening, and closing an image. In an image, the pixels are added to the boundaries of the objects by dilation and removed on object boundaries by erosion. The size and shape of the structuring element in image processing are the critical variables for the number of pixels added or removed from the objects in an image. Applying a rule to the corresponding pixel and its neighbors in an input image determines any given pixel in the output image in the morphological dilation and erosion operations.

Moreover, two critical operators of mathematical image morphology are opening and closing. The fundamental operations are used to derive them following erosion and dilation. The opening, together with closing, serves as a useful step for noise removal in image processing and computer vision. Some of the bright pixels from the edges of regions of foreground pixels are removed by opening. Closing tends to enlarge foreground regions' boundaries in an image similar to dilation to shrink background color holes in such areas. It still manages to be less destructive of the original boundary shape.

Our study has applied morphological image processing to the grayscale UAV images derived from the Micasense Red edge camera with 5-bands to extract their relevant tree detection components. We have extended the morphological operations to grayscale images using minimum and maximum filtering attributed to each image pixel a new value equal to the minimum or maximum value in a neighborhood around that pixel.

At the first step, the grayscale dilation was assigned to each pixel the maximum value found over the neighborhood of the structuring element for growing image regions by the Eq. (4):

$$\delta_B(f)_x = (f \oplus B)_x = \max_{\beta \in B} (x + \beta) \quad (4)$$

where x is the dilated value of a pixel, $S.E.$: the maximum value of the image in the neighborhood when its origin is at x , after the dilation, the grayscale erosion was applied by assigning to each pixel the minimum value for shrinking image regions (Eq. (5)).

$$\epsilon_B(f)_x = (f \ominus B)_x = \min_{\beta \in B} (x + \beta) \quad (5)$$

The eroded value of a pixel x is the minimum value of the neighborhood's image defined by the Structuring Element (SE) when its origin is at x (Zaoui and Belmadani, 2021). After the erosion, the grayscale opening of an image was performed for the structured removal of image region boundary pixels. The opened value of a pixel is the maximum of the minimum value of the image in the neighborhood defined by the SE . Moreover, the grayscale closing of an image was performed for structured filling in image region boundary pixels (Adams and Bischof, 1994). The opening of set X by structuring element B , denoted $X \circ B$, is defined as (*Opened Image*) (Eq. (6)), and the opening of set X by structuring element B , denoted $X \bullet B$, is defined as (*Closed Image*) (Eq. (7)):

$$\text{Opened Image} = XB = (X - B) + B \quad (6)$$

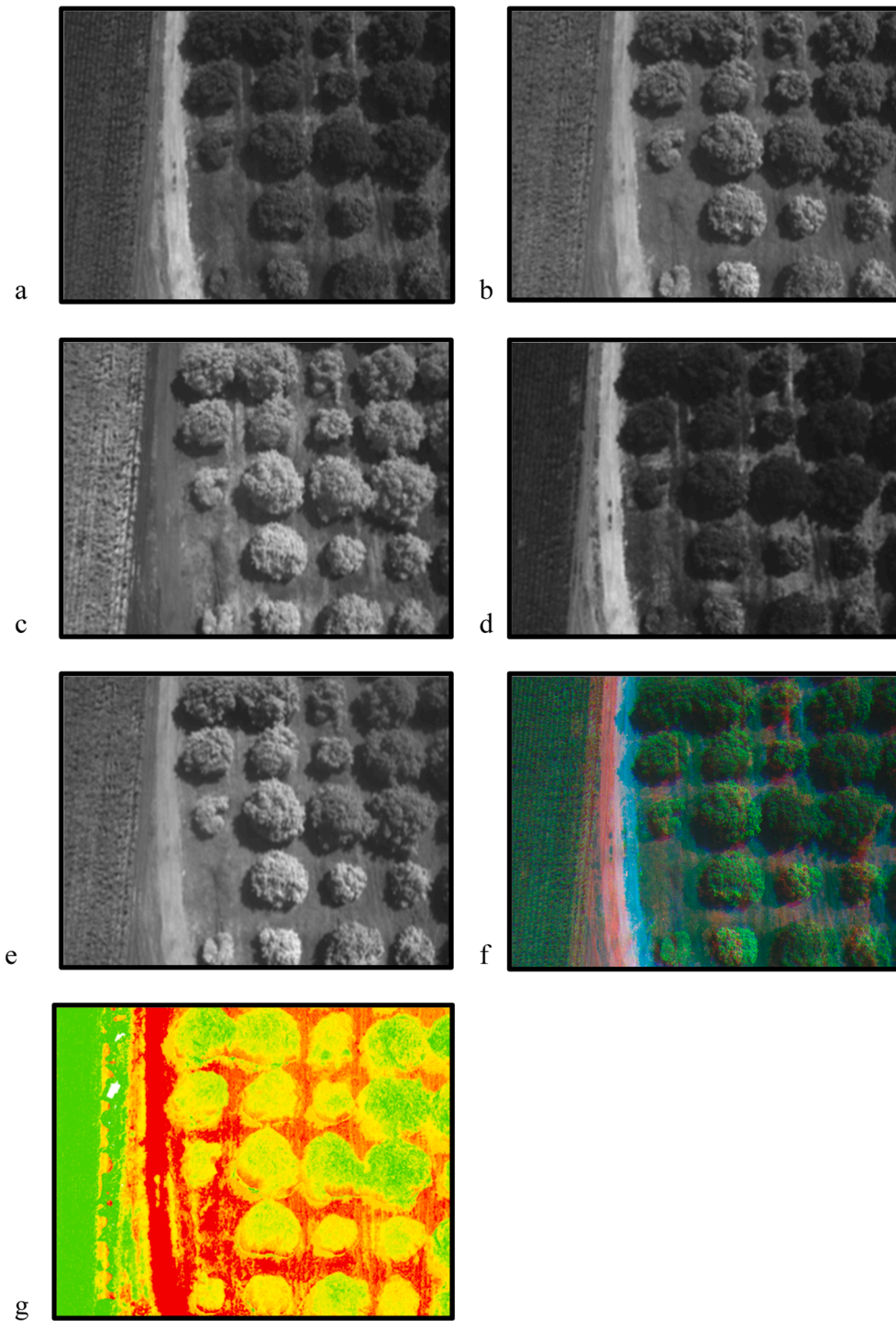


Fig. 7. Sample subsets of the Blue (a), Green (b), Near-IR (c), Red (d), and Red Edge (e) and bands acquired by the DJI V8 octocopter and Micasense Red edge camera from patch 2 in the study site (f) comprises the RGB image derived using MATLAB, (g) NDVI. (For interpretation of the references to color in this figure legend, the reader is referred to the web version of this article.)

$$Closed\ Image = XB = (X + B) - B \tag{7}$$

Following the compound analysis, we have converted the morphologically processed grayscale images (for each spectral band) to a binary format to include the CCL workflow (Eq. (8)).

$$Image_{ij} = \begin{cases} max_val, & Image(i,j) > 0 \\ 0, & else \end{cases} \tag{8}$$

Thresholding is an effective method in image processing for image

segmentation and creating binary images from grayscale images. We used automated thresholding to minimize background noise for extracting required objects (e.g. trees) from the images. Once the edges were detected, the treed regions less than < 50 pixels were removed for decreasing the noise. Automated thresholding was based on the object-attribute method as one of the histogram shape-based methods. It allowed multiband thresholding, including grayscale and colored images used in the study, to make certain assumptions in image intensities for object extraction in better accuracy (Sezgin and Sankur, 2004).

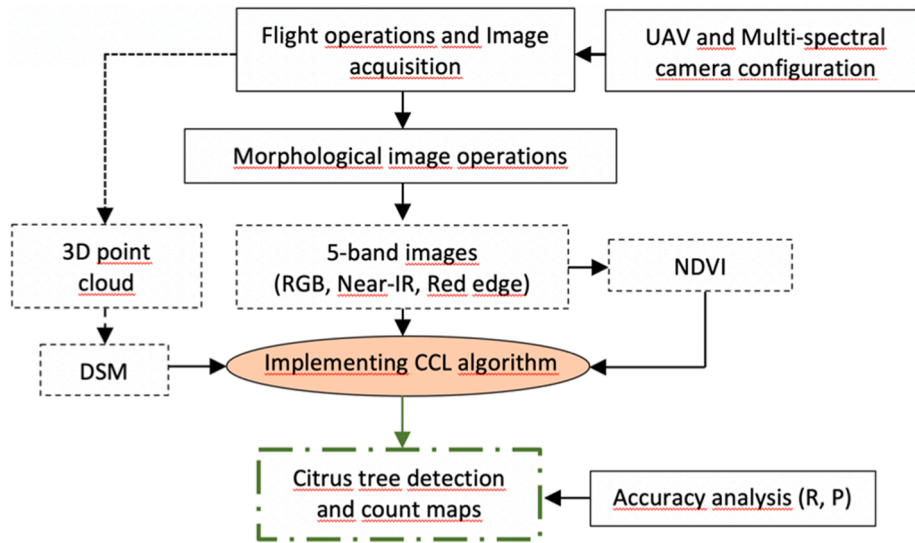


Fig. 8. Flow diagram of the study.

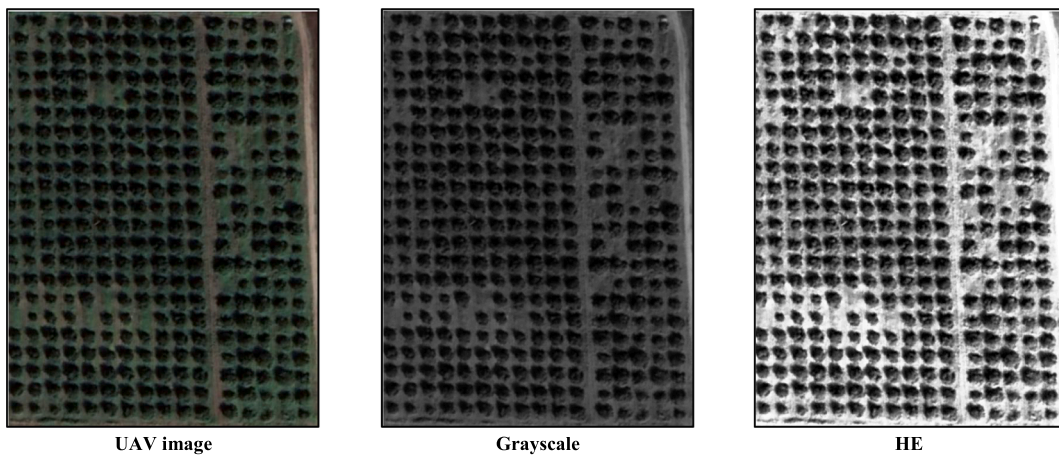


Fig. 9. Contrast distribution of the UAV and grayscale images as well as HE.

Hence, we applied thresholding to each band by dividing the images into two sides: background and foreground. A feedback loop was employed for weighting the histogram between the two sides and repeated it for each band until the edges of the weighting scale meet (Anjos and Shahbazkia, 2008).

After detecting the tree regions, they were localised in each row of the orchard. The distance between the tree regions in a row was calculated using a Euclidean distance algorithm. Transformations of the acquired UAV images applying the morphological image operations to include the CCL workflow are given in Fig. 10 based on the automated thresholding.

3.3. Detection and counting citrus trees with a CCL workflow

After completing the morphological operations, we have employed a CCL algorithm to detect and count the citrus trees in binary images in a sequential labeling way. It was detecting and counting the operation of the label-connected components. Our approach detected the connected components between the pixels in the binary formats of our input images, including DEM, Red, Green, Blue, Near-IR, Red edge bands, and NDVI converted from the grayscale images. The sequential labeling algorithm we used in our study is a non-recursive technique that identifies the connected components of an image. It scans an image pixel basis and

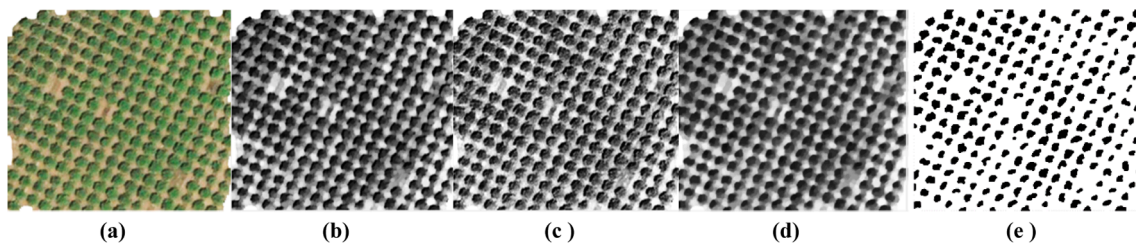


Fig. 10. Transformation of the acquired UAV images by the morphological operations for the CCL workflow; (a) acquired, (b) opened, (c) grayscale and HE, (d) closed, (e) binary.

then assigns a label to each object based on the neighbourhood (4, 6, or 8-connectivity) with a two scan process.

Our study employed 8-connected (N8) neighbourhood to our binary input images and labeled their pixels in each direction in the scanning mask. In this process, the algorithm scanned a pixel and examined its neighbours in the mask for an appropriate label determination for the object pixel. All neighbours ($N1 = b(x, y-1)$, $N2 = b(x-1, y-1)$, $N3 = b(x-1, y)$ and $N4 = b(x-1, y + 1)$) were examined as $b(x,y)$ (Dharpure et al., 2013) (Fig. 11).

The two-scan algorithm (Shapiro and Stockman, 2001) based on the CCL iterated through the binary format and passed twice over the image. The 8-connected sequential region labeling algorithm used in our study is illustrated in Fig. 12.

While obtaining images in first and second scans from the binary image, we scanned the binary image pixel by pixel in all four directions (left–right, top–bottom). We assigned a temporary provisional label in the first scan by marking the foreground pixel of the binary image as 1 while background pixels as 0. First, a number of the object by zero were initialized. If the equivalent array value is equal to integer number one, the number of objectives were increased and replaced with the representative label. Otherwise, no change has occurred in the equivalent array value. Thus, a representative label was produced, and it was merged with each connected component in the binary image to create unique labels through the equivalence table (Chabardès et al., 2020) in the second scan. If the 1 representative label and object labels are the same, the labels are not changed in the image. If the labels are different, a new label is assigned to the object pixel (trees) from a representative set. At the end of the scanning process, each connectivity component in the image is assigned a unique label described in Dharpure et al. (2013) and Charbardes et al. (2020).

After labeling and detecting the object (citrus trees) pixels, they were counted by a one-dimensional representative array. Several objects were initialized by zero first. When the array value was an integer, the number of objects increased, and the label value was replaced. This process continued until the entire object on the images was recognized and counted.

3.4. Validation

Evaluating the results of the CCL algorithms is necessary to validate the outputs, however always a challenging task due to their data dependency. We used a reference tree dataset collected from the study sites for validation. The reference data set comprised the number of the trees and their species and focussed on the detected number of citrus trees and the existing ones in the study site. The coordinates of reference for each tree were recorded using a GPS in field campaigns to compare detected tree information from the UAV images. Besides, bush diameters of these citrus trees were also measured using a laser meter to provide an ancillary reference set for comparing the segmented tree outputs from the image morphological operations. A buffer around these tree-based point samples was derived as suggested in Csillik et al., (2018). In this case, the bush diameter of each tree was represented by around 100 pixels, and the regression has chosen their presence out of these pixels for validation.

Each citrus tree detected and counted by the CCL was compared to its closest existing tree on the images by common evaluation statistics for binary classification (Saito and Rehmsmeier, 2015). We computed correctly identified trees as True Positives (TP), incorrectly identified as

False Positives (FP), and missing trees (MT). The relationship between these variables indicated a successful, over, or under-identification. Recall ($R = TP/TP + MT$) was calculated to accurately describe the tree detection rate based on these indicators. The accuracy of the tree counting and detection was revealed with overall R and also Precision (P) ($TP/(TP + FP)$) outputs (Csillik et al., 2018).

4. Results and discussion

A comprehensive approach combining sequential CCL algorithm and morphological image operations was employed in a UAV image set to detect and count the orchard citrus trees in the experiment. The study site was tracked in two parts as patch-1 and patch-2, and the UAV images were acquired for both sites. In both patches, three species were defined (Washington Navel, Fukumoto, Navelina) that were planted in 34 (patch-1) and 24 (patch-2) rows. These rows mostly have one species, and only a few have an order of mixed oranges.

In total, 1560 UAV images were acquired and processed using the 8-connected CCL methodology. These images were converted to binary format and used in tree detection and counting. An example of citrus tree detection of the binary image for patch 2 is shown in Fig. 13.

The coloured segmentation of the citrus trees indicated a detection on the binary imagery with a diameter of 2.5 m, and these trees were counted as full-grown. Additionally, the detected and counted citrus trees in patch 1 are illustrated on the UAV-derived Red Edge, Near-IR, NDVI, and DSM in Fig. 14.

Red and Green bands resulted in inaccurate tree recognition relative to the other bands and the DSM. These bands provided insufficient contrast for tree detection in shaded canopies contrary to Red edge and Near-IR. Besides, it was seen that the citrus trees and bare ground with even sparse grasses showed close surface reflectances at especially in the green band. It might be assumed an adverse effect of the CCL performance with the mentioned band.

Although the sequential CCL methodology struggled in the Red and Green bands, incorporating them into the morphological image operations provided promising results for detecting and counting citrus trees in a Mediterranean orchard for the proposed task. In field campaigns, 1506 citrus trees were counted and recorded manually for validating the CCL outputs over the UAV imagery. 956 citrus trees with mixed species were counted for the patch-1, and 550 trees for the patch-2. The fixed window size was taken into account as 3x3 in the 8-connected CCL process. Table 3 shows the tree detection and counting performance of the CCL methodology for each UAV band, NDVI, and DSM set.

The results indicated that the 8-connected sequential CCL algorithm performance was remarkable for detecting and counting the citrus tree sizes from high-resolution UAV imagery. It dealt with the heterogeneous tree sizes within the patches effectively and detected the various canopy sizes with reasonable accuracy. A total of 1462 citrus trees (mean value) were detected and compared to the reference tree set. The number of T. P. was 62, and MT was 30 on average. DSM showed the highest performance in tree detection with 1484 TP, 34 FP, and 11 MT. Some refinements are needed with the Green band, which could barely detect the small crown trees. The overall R accuracy of the CCL methodology was 0,979 with a P of 0,959. The use of DSM and Red-Edge bands provided the best results.

The citrus trees of patch 1 are well grown and homogeneous as well the patch 2. There are only a few gaps detected on their rows. We realized that our CCL technique detected trees with 2.5 m diameter systematically. The method was also successful in avoiding the tree gaps and seedlings of the plantation rows

The results show that citrus plantation lines are also identified from the CCL approach without any additional procedure. This is especially important for precision agriculture and related remote sensing applications to assist missing tree detection, crop rotation, and optimization (do Nascimento Oliveira et al., 2018). However, there were also many challenges faced during the conducted segmentation for tree

$b(x-1, y-1)$	$b(x-1, y)$	$b(x-1, y+1)$
$b(x, y-1)$	$b(x,y)$	$b(x, y+1)$
$b(x+1, y-1)$	$b(x+1, y)$	$b(x+1, y+1)$

Fig. 11. 8-connected connectivity neighbourhood of pixel $b(x, y)$.

1	0	0	0	1	1	0	0	1	1	0	0	0	1	2	0	0	4	1	0	0	0	1	1	0	0	2
1	0	0	1	1	1	0	0	1	2	0	0	1	1	1	0	0	4	1	0	0	1	1	1	0	0	2
0	0	1	1	1	0	0	0	0	0	0	1	1	1	0	0	0	0	0	0	1	1	1	0	0	0	0
0	0	0	1	1	0	0	1	1	0	0	0	1	1	0	0	3	4	0	0	0	1	1	0	0	2	2
0	0	0	0	0	0	1	1	1	0	0	0	0	0	0	3	3	3	0	0	0	0	0	0	2	2	2
0	0	1	0	0	0	1	1	1	0	0	5	0	0	0	3	3	3	0	0	3	0	0	0	2	2	2
1	1	1	0	0	0	0	0	0	5	5	5	0	0	0	0	0	0	3	3	3	0	0	0	0	0	0
1	1	0	0	0	0	0	0	0	5	5	0	0	0	0	0	0	0	3	3	0	0	0	0	0	0	0
1	1	0	0	1	1	1	0	0	5	5	0	0	3	3	3	0	0	3	3	0	0	2	2	2	0	0
i									ii									iii								

Fig. 12. Sample of the 8-connected sequential CCL algorithm used in the study site (binary image (i), first scan (ii), second scan (iii)).

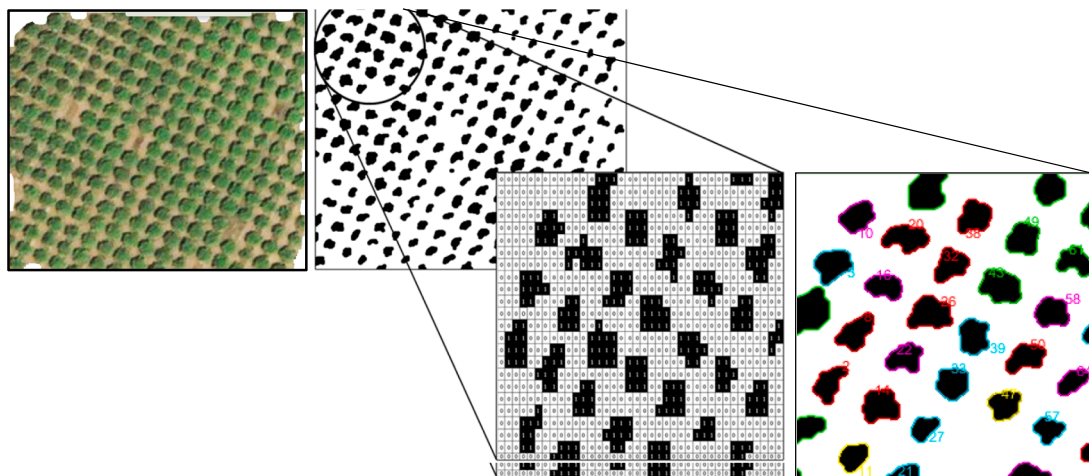


Fig. 13. Examples of the RGB (left) and binary image (middle), as well as the detected citrus trees (labeled (left) and segmented (right)) (1 indicates citrus pixels and 0 showed non-citrus pixels).

recognition. An example of recognition error in the CCL approach is presented in Fig. 15.

A sufficient number of ground truth data were collected to perform an accuracy analysis of the algorithm. The results from this study are comparable with similar studies that included tree recognition and detection using UAV images. Nevalainen et al. (2017) detected individual trees in the forest environment using hyperspectral imagery from a UAV and examined a similar number of trees comparable to our study. Wallace et al. (2014) and Zhen et al. (2016) applied a tree crown detection methodology using LIDAR with high precision. Sperlich et al. (2014) derived point clouds using a pouring algorithm from UAV-based aerial photos and detected trees with 87.68% accuracy. Kattenborn et al. (2014) improved the pouring algorithm to classify the point clouds geometrically and detected palm trees with an 86.1% accuracy in a dense orchard. Similar results with our study were reported in Csillik et al. (2018), Mohan et al. (2017), and Lim et al. (2015). Addressing these studies, our study is the first to use CCL on the multi-spectral UAV imagery to succeed remarkable accuracy for individual citrus tree detection.

The results indicated that our CCL approach was able to extract the full-grown trees successfully. However, additional improvements could be needed to detect the younger trees that appeared with lower frequency. The mentioned lower frequency brought difficulty to separate the tree bushes and shadow effects. In this respect, increasing the ground samples and including a training set could bring an advantage for improved detection of trees.

The challenges related to tree recognition were mainly addressed to the tree characteristics, shadow effects, and short planting lines.

Presenting much of the canopy occurred a confusion on the approach to differentiating tree centroids. However, even much canopy appeared, the proposed methodology was capable of recognizing the location of the trees. Even though there were missing trees removed due to spacing and health issues, the plantation lines with reasonably spaced trees were defined by the sequential CCL remarkably. Overall, the proposed methodology was able to detect the regular planting lines and citrus trees successfully. These outcomes indicated the suitability of the two-scan CCL for predicting orchard trees, even with gaps in the planting lines.

5. Conclusions

Common methods for feature extraction (ANNs, object-based image analysis, etc.) require a large dataset for training for extracting the individual trees. Besides, they can also struggle to cope with multiscale objects and landscapes with diverse spatial patterning. Our study presented a comprehensive framework for developing an automated tree counting and detection from a UAV imagery CCL based algorithm designed for multi-spectral image processing, which does not require large training datasets. We employed an 8-connected and two scan CCL algorithm to extract the citrus trees accurately and overcome the scale problems (age and shape variations of the trees). Our work can be realized as an essential example for using the CCL algorithms incorporating UAV imagery and morphological operations to increase the ability of automated tree recognition processes for agricultural purposes. It comprises a high potential to provide an efficient, cost-effective, and accurate approach for object detection to support

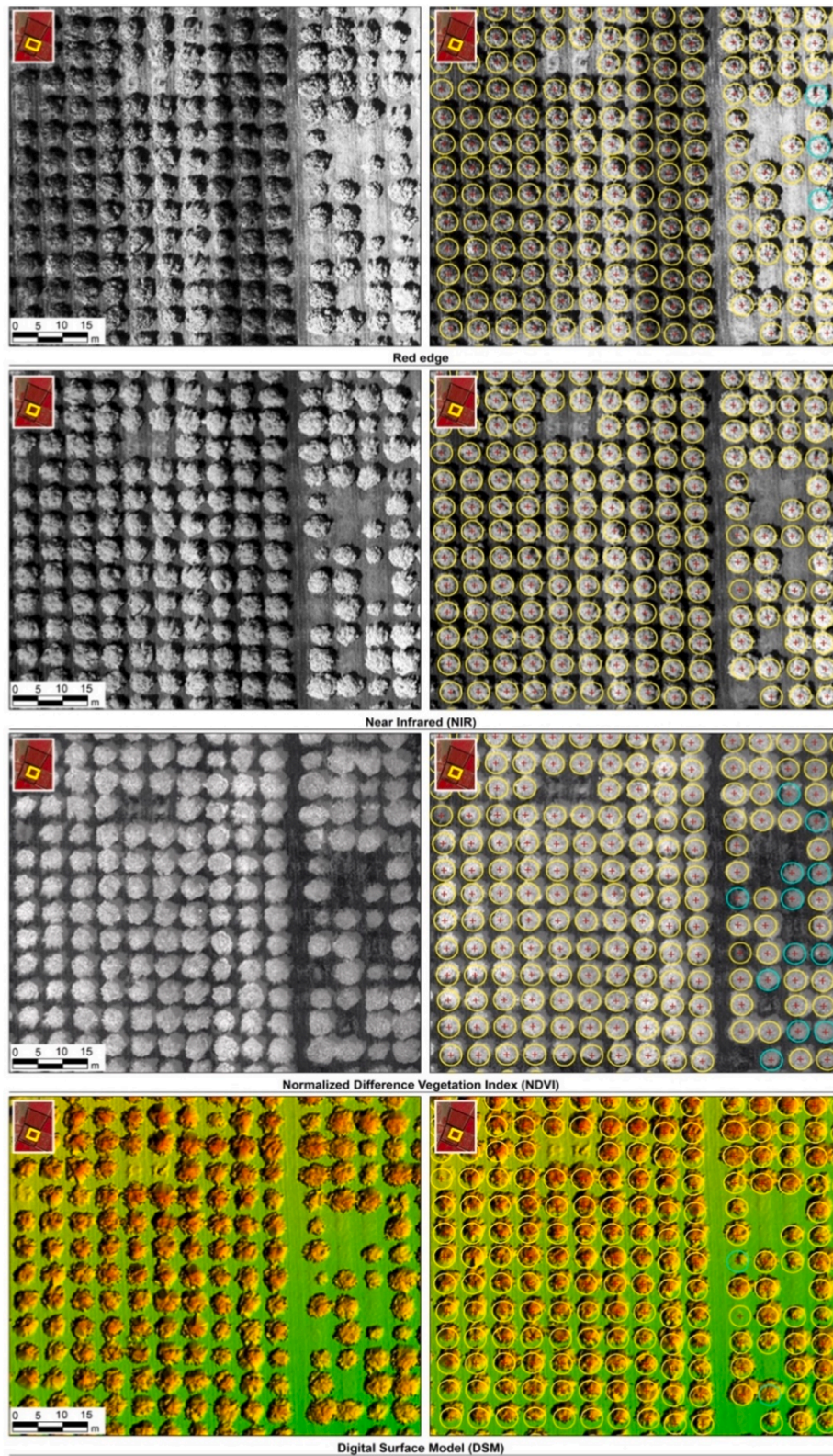


Fig. 14. Examples of identified citrus trees from the UAV-derived Red edge, Near-IR, NDVI, and DSM using the 8-connected CCL algorithm.

agricultural monitoring and crop management.

The success of similar studies depended not only on the methodology but also on the physical and environmental conditions. For instance, the UAV systems have many challenges, including weather conditions, flying height, and camera specifications compared to satellite platforms. These challenges can affect the efficiency of its quality data supply to use

subsequent agricultural analysis. Therefore, we have given a considerable effort and focus on developing an equipmentally compatible and efficient UAV platform. During the process, we recognized that the battery voltage used in the octocopter was not within a safe range for operating the Micasense camera, which was five volts. Thus, we integrated a voltage regulator to provide a safe range and also implemented

Table 3

Citrus tree detection performance of the CCL method applied to the UAV images.

Bands/ Images	Number of trees			Recall	Precision
	True positives (TP)	False positives (FP)	Missing trees (MT)		
Red band	1456	70	35	0,977	0,954
Green band	1448	82	45	0,970	0,946
Blue Band	1461	60	36	0,976	0,961
Near-IR	1469	42	32	0,979	0,972
Red Edge	1474	46	27	0,982	0,970
NDVI	1444	102	27	0,982	0,934
DSM	1484	34	11	0,993	0,978

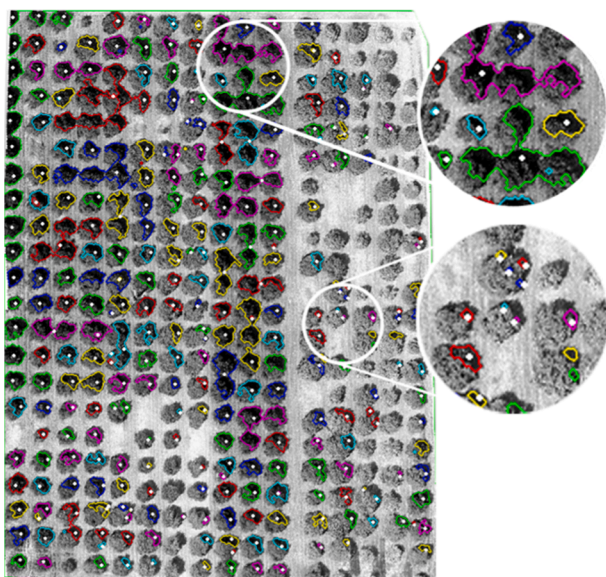


Fig. 15. An example of recognition error in the CCL approach.

an XT-60 multiplier connector into the battery. Besides, the number of engines is also an essential point for the flight safety and rotation capability of the UAV. The engine settings should be done and installed on the flight controller for a safe flight.

Despite the importance and advantages of UAV-based systems and methods, multidisciplinary UAV remote sensing applications are still limited. Research attempts should especially be increasingly focussed on forest and agricultural studies. Formulating approaches to optimize tree recognition, detection, and counting related algorithms would provide insights into UAV integration into the agriculturally and forest-related analytics. The goal of imposing a CCL algorithm in our study is to reveal a satisfactory solution that is low-cost, scalable and compatible with UAV-based studies. We derived encouraging outputs to demonstrate the potential of UAV-based multi-spectral imagery, computer-vision algorithms and photogrammetric point clouds for agricultural studies and orchard management. It suggests that the CCL, as a computer-vision algorithm, can detect and count different-sized (young or full-growth) citrus trees in complex agricultural patches with reasonable accuracy. The work can be extended to cover larger areas for efficient yield predictions, especially for the Mediterranean regions with high citrus cultivation.

Moreover, further research could comprise the 3D analysis and different connection levels (4, 6-connected) in a two-pass labeling process to reveal the efficiency of these processes with UAV imagery. It could be extended to the extraction of different crops (i.e., corn, maize, soya), which could provide a considerable advantage for agricultural

management and monitoring. Addressing our study's outputs, UAV-based research directions for the future could identify the tree species and percent tree cover that are significant factors for yield and diameter estimations.

Funding

This research was funded by the Turkish Scientific and Research Council (TUBITAK) with grant number 115Y063.

CRedit authorship contribution statement

Genk Donmez: Conceptualization, Methodology, Writing - original draft. **Osman Villi:** Data curation, Methodology, Software. **Suha Berberoglu:** Methodology, Writing - review & editing. **Ahmet Cilek:** Software, Validation.

Declaration of Competing Interest

The authors declare the following financial interests/personal relationships which may be considered as potential competing interests: Suha Berberoglu reports financial support was provided by Turkish Scientific and Research Council (TUBITAK).

Acknowledgments

This research was funded by the Turkish Scientific and Research Council (TUBITAK) (Project grant number: 115Y063)

References

- Acharya, T., Ray, A.K., 2005. Image Processing: Principles and Applications, Image Processing: Principles and Applications. John Wiley & Sons, Inc., Hoboken, NJ, USA. <https://doi.org/10.1002/0471745790>.
- Adams, R., Bischof, L., 1994. Seeded region growing. *IEEE Trans. Pattern Anal. Mach. Intell.* 16, 641–647. <https://doi.org/10.1109/34.295913>.
- Al Mansoori, S.H., Kunhu, A., Al Ahmad, H., 2018. Automatic palm trees detection from multispectral UAV data using normalized difference vegetation index and circular Hough transform. p. 3. <https://doi.org/10.1117/12.2325732>.
- Ampatzidis, Y., Partel, V., 2019. UAV-based high throughput phenotyping in citrus utilizing multispectral imaging and artificial intelligence. *Remote Sens.* 11, 410. <https://doi.org/10.3390/rs11040410>.
- Anjos, A., Shahbazkia, H., 2008. Bi-level image thresholding - a fast method. *Biosignals* 2, 70–76.
- Aplin, P., 2004. Remote sensing: Land cover. *Prog. Phys. Geogr.* 28, 283–293. <https://doi.org/10.1191/0309133304pp413pr>.
- Belgiu, M., Csillik, O., 2018. Sentinel-2 cropland mapping using pixel-based and object-based time-weighted dynamic time warping analysis. *Remote Sens. Environ.* 204, 509–523. <https://doi.org/10.1016/j.rse.2017.10.005>.
- Campos, Y., Sossa, H., Pajares, G., 2016. Spatio-temporal analysis for obstacle detection in agricultural videos. *Appl. Soft Comput.* 45, 86–97.
- Campos, Y., Sossa, H., Pajares, G., 2017. Comparative analysis of texture descriptors in maize fields with plants, soil and object discrimination. *Precis. Agric.* 18 (5), 717–735.
- Celik, T., 2009. Unsupervised change detection in satellite images using principal component analysis and κ -means clustering. *IEEE Geosci. Remote Sens. Lett.* 6, 772–776. <https://doi.org/10.1109/LGRS.2009.2025059>.
- Chabardès, T., Dokládal, P., Bilodeau, M., 2020. A labeling algorithm based on a forest of decision trees. *J. Real-Time Image Process.* 17, 1527–1545. <https://doi.org/10.1007/s11554-019-00912-8>.
- Chen, S.W., Shivakumar, S.S., Dcunha, S., Das, J., Okon, E., Qu, C., Taylor, C.J., Kumar, V., 2017. Counting apples and oranges with deep learning: a data-driven approach. *IEEE Robot. Autom. Lett.* 2, 781–788. <https://doi.org/10.1109/LRA.2017.2651944>.
- Cilek, A., Berberoglu, S., Akça, E., Donmez, C., Erdogan, M.A., Kapur, B., Kapur, S., 2020. Soil Degradation: Global Assessment, in: Jørgensen, B.D.F. and S.E. (Ed.), *Managing Soils and Terrestrial Systems Second Edition*. CRC Press, pp. 217–234.
- Csillik, O., Cherbini, J., Johnson, R., Lyons, A., Kelly, M., 2018. Identification of citrus trees from unmanned aerial vehicle imagery using convolutional neural networks. *Drones* 2, 1–16. <https://doi.org/10.3390/drones2040039>.
- Deng, L., Mao, Z., Li, X., Hu, Z., Duan, F., Yan, Y., 2018. UAV-based multispectral remote sensing for precision agriculture: A comparison between different cameras. *ISPRS J. Photogramm. Remote Sens.* 146, 124–136. <https://doi.org/10.1016/j.isprsjprs.2018.09.008>.
- Diani, M., Corsini, G., Baldacci, A., 2001. Space-time processing for the detection of airborne targets in IR image sequences, in: *IEE Proceedings: Vision, Image and Signal Processing*. pp. 151–157. <https://doi.org/10.1049/ip-vis:20010308>.

- Díaz-Varela, R.A., de la Rosa, R., León, L., Zarco-Tejada, P.J., 2015. High-resolution airborne UAV imagery to assess olive tree crown parameters using 3D photo reconstruction: Application in breeding trials. *Remote Sens.* 7, 4213–4232. <https://doi.org/10.3390/rs70404213>.
- Djerriri, K., Ghabi, M., Karoui, M.S., Adjoudj, R., 2018. Palm trees counting in remote sensing imagery using regression convolutional neural network. *Int. Geosci. Remote Sens. Symposium (IGARSS)*. 2627–2630. <https://doi.org/10.1109/IGARSS.2018.8519188>.
- Dharpure, J.K., Potdar, M.B., Pandya, M., 2013. Counting objects using homogeneous connected components. *Int. J. Comput. Appl.* 63, 31–37. <https://doi.org/10.5120/10590-5585>.
- do Nascimento Oliveira, A., de Almeida Paula, D., Basílio de Oliveira, E., Henriques Saraiva, S., Stringheta, P.C., Mota Ramos, A., 2018. Optimization of pectin extraction from Ubá mango peel through surface response methodology. *Int. J. Biol. Macromol.* 113, 395–402. <https://doi.org/10.1016/j.ijbiomac.2018.02.154>.
- Donmez, C., Berberoglu, S., Erdogan, M.A., Tanriover, A.A., Cilek, A., 2015. Response of the regression tree model to high resolution remote sensing data for predicting percent tree cover in a Mediterranean ecosystem. *Environ. Monit. Assess.* 187, 4.
- Golland, P., Bruckstein, A.M., 1996. Why RGB? Or how to design color displays for Martians. *Graphical Models and Image Processing* 58 (5), 405–412.
- Hall, O., Dahlin, S., Marstorp, H., Bustos, M.F.A., Öborn, I., Jirstrom, M., 2018. Classification of maize in complex smallholder farming systems using UAV imagery. *Drones* 2, 1–8. <https://doi.org/10.3390/drones2030022>.
- He, L., Chao, Y., Suzuki, K., 2012. A new two-scan algorithm for labeling connected components in binary images. *Lecture Notes in Engineering and Computer Science* 1141–1146.
- Hentschke, M., de Freitas, E.P., Hennig, C.H., da Veiga, I.C.G., 2018. Evaluation of altitude sensors for a crop spraying drone. *Drones* 2, 1–16. <https://doi.org/10.3390/drones2030025>.
- Hunt, E.R., Daughtry, C.S.T., 2018. What good are unmanned aircraft systems for agricultural remote sensing and precision agriculture? *Int. J. Remote Sens.* 39, 5345–5376. <https://doi.org/10.1080/01431161.2017.1410300>.
- Jain, A.K.,atha, N.K., Lakshmanan, S., 1997. Object detection using Gabor filters. *Pattern Recognit.* 30, 295–309. [https://doi.org/10.1016/S0031-3203\(96\)00068-4](https://doi.org/10.1016/S0031-3203(96)00068-4).
- Jiang, H., Chen, S., Li, D., Wang, C., Yang, J., 2017. Papaya tree detection with UAV images using a GPU-accelerated scale-space filtering method. *Remote Sens.* 9, 721. <https://doi.org/10.3390/rs9070721>.
- Kattenborn, T., Sperlich, M., Bataua, K., Koch, B., 2014. Automatic single palm tree detection in plantations using UAV-based photogrammetric point clouds. *Int. Arch. Photogramm. Remote Sens. Spat. Inf. Sci. - ISPRS Arch.* 40, 139–144. <https://doi.org/10.5194/isprsarchives-XL-3-139-2014>.
- Lim, Y.S., La, P.H., Park, J.S., Lee, M.H., Pyeon, M.W., Kim, J.I., 2015. Calculation of tree height and canopy crown from drone images using segmentation. *J. Korean Soc. Surv. Geod. Photogramm. Cartogr.* 33, 605–613. <https://doi.org/10.7848/kgspc.2015.33.6.605>.
- Lin, Y., Peng, Y., Wenyang, H., et al., 2019. Detection of anthracnose in tea plants based on hyperspectral imaging. *Comput. Electron. Agric.* 167, 105039. <https://doi.org/10.1016/j.compag.2019.105039>.
- Maded, S., Jin, X., Lu, H., De Solan, B., Liu, S., Duyme, F., Heritier, E., Baret, F., 2019. Ear density estimation from high resolution RGB imagery using deep learning technique. *Agric. For. Meteorol.* 264, 225–234. <https://doi.org/10.1016/j.agrformet.2018.10.013>.
- Malek, S., Bazi, Y., Alajlan, N., AlHichri, H., Melgani, F., 2014. Efficient framework for palm tree detection in UAV images. *IEEE J. Sel. Top. Appl. Earth Obs. Remote Sens.* 7, 4692–4703. <https://doi.org/10.1109/JSTARS.2014.2331425>.
- Mattos, A.B., Zortea, M., Macedo, M.M.G., Ruga, B.C., Gemignani, B.H., 2018. Automatic Citrus Tree Detection from UAV Images based on Convolutional Neural Networks Intravascular Optical Coherence Tomography image analysis View project Automatic Citrus Tree Detection from UAV Images based on Convolutional Neural Networks, in: Conference: 31th Sibgrap/WIA - Conference on Graphics, Patterns and Images.
- Micasense, 2015. MicaSense RedEdge TM 3 Multispectral Camera User Manual.
- Miller, D.M., Kaminsky, E.J., Rana, S., 1995. Neural network classification of remote-sensing data. *Comput. Geosci.* 21, 377–386. [https://doi.org/10.1016/0098-3004\(94\)00082-6](https://doi.org/10.1016/0098-3004(94)00082-6).
- Mohan, M., Silva, C.A., Klauber, C., Jat, P., Catts, G., Cardil, A., Hudak, A.T., Dia, M., 2017. Individual tree detection from unmanned aerial vehicle (UAV) derived canopy height model in an open canopy mixed conifer forest. *Forests* 8, 340. <https://doi.org/10.3390/f8090340>.
- Mountrakis, G., Im, J., Ogole, C., 2011. Support vector machines in remote sensing: A review. *ISPRS J. Photogramm. Remote Sens.* 66, 247–259. <https://doi.org/10.1016/j.isprsjprs.2010.11.001>.
- NCA, 2020. National Citrus Association of Turkey [WWW Document]. Off. Web Site, <http://utk.org.tr/>.
- Nevalainen, O., Honkavaara, E., Tuominen, S., Viljanen, N., Hakala, T., Yu, X., Hyypää, J., Saari, H., Pölonen, I., Imai, N.N., Tommaselli, A.M.G., 2017. Individual tree detection and classification with UAV-Based photogrammetric point clouds and hyperspectral imaging. *Remote Sens.* 9. <https://doi.org/10.3390/rs9030185>.
- Pix4D, 2018. Available online: <https://pix4d.com/> (accessed on 7 August 2018).
- Oscro, L.P., de Arruda, M. dos S., Marcato Junior, J., da Silva, N.B., Ramos, A.P.M., Moryia, É.A.S., Imai, N.N., Pereira, D.R., Creste, J.E., Matsubara, E.T., Li, J., Gonçalves, W.N., 2020. A convolutional neural network approach for counting and geolocating citrus-trees in UAV multispectral imagery. *ISPRS J. Photogramm. Remote Sens.* 160, 97–106. <https://doi.org/10.1016/j.isprsjprs.2019.12.010>.
- Ozdarici-Ok, A., 2015. Automatic detection and delineation of citrus trees from VHR satellite imagery. *Int. J. Remote Sens.* 36, 4275–4296. <https://doi.org/10.1080/01431161.2015.1079663>.
- Ramesh, K.N., Chandrika, N., Omkar, S.N., Meenavathi, M.B., Rekha, V., 2016. Detection of rows in agricultural crop images acquired by remote sensing from a UAV. *Int. J. Image Graph. Signal Process.* 8, 25–31. <https://doi.org/10.5815/ijgisp.2016.11.04>.
- Saito, T., Rehmsmeier, M., 2015. The precision-recall plot is more informative than the ROC plot when evaluating binary classifiers on imbalanced datasets. *PLoS ONE* 10 (3), e0118432. <https://doi.org/10.1371/journal.pone.0118432>.
- Satir, O., Berberoglu, S., Donmez, C., 2016. Mapping regional forest fire probability using artificial neural network model in a Mediterranean forest ecosystem. *Geomatics. Nat. Hazards Risk* 7, 1645–1658. <https://doi.org/10.1080/19475705.2015.1084541>.
- Sezgin, M., Sankur, B., 2004. Survey over image thresholding techniques and quantitative performance evaluation. *J. Electron. Imaging* 13 (1), 146–165.
- Shapiro, L.G., Stockman, G., 2001. *Computer Vision*. Upper Saddle River, Pearson Education, p. 608p.
- Sperlich, M., Kattenborn, T., Koch, B., Kattenborn, G., 2014. Potential of Unmanned Aerial Vehicle Based Photogrammetric Point Clouds for Automatic Single Tree Detection. *Gemeinsame Tagung, 2014 der DGfK, der DGPF, der GfGI und des GIN* 1–6.
- Surovyy, P., Almeida Ribeiro, N., Panagiotidis, D., 2018. Estimation of positions and heights from UAV-sensed imagery in tree plantations in agrosilvopastoral systems. *Int. J. Remote Sens.* 39, 4786–4800. <https://doi.org/10.1080/01431161.2018.1434329>.
- Thyagarajan, K.K., Vignesh, T., 2019. Soft Computing Techniques for Land Use and Land Cover Monitoring with Multispectral Remote Sensing Images: A Review. *Archives of Computational Methods in Engineering*, 26. Springer Publication, pp. 275–301. <https://doi.org/10.1007/s11831-017-9239-y>.
- Thyagarajan, K.K., Kiruba Raji, I., 2019. A review of visual descriptors and classification techniques used in leaf species identification. *Arch. Computat. Methods Eng.* 26, 933–960. <https://doi.org/10.1007/s11831-018-9266-3>.
- Torres-Sánchez, J., López-Granados, F., Serrano, N., Arquero, O., Peña, J.M., 2015. High-throughput 3-D monitoring of agricultural tree plantations with Unmanned Aerial Vehicle (UAV) technology. *PLoS ONE* 10. <https://doi.org/10.1371/journal.pone.0130479>.
- Vazquez-Nicolas, J.M., Zamora, E., González-Hernández, I., Lozano, R., Sossa, H., 2020. PD+SMC quadrotor control for altitude and crack recognition using deep learning. *Int. J. Control Autom. Syst.* 18, 834–844. <https://doi.org/10.1007/s12555-018-0852-9>.
- Verma, N.K., Lamb, D.W., Reid, N., Wilson, B., 2016. Comparison of canopy volume measurements of scattered eucalypt farm trees derived from high spatial resolution imagery and LiDAR. *Remote Sens.* 8. <https://doi.org/10.3390/rs8050388>.
- Wallace, L., Lucieer, A., Watson, C.S., 2014. Evaluating tree detection and segmentation routines on very high resolution UAV LiDAR data. *IEEE Trans. Geosci. Remote Sens.* 52, 7619–7628. <https://doi.org/10.1109/TGRS.2014.2315649>.
- Yang, C., 2020. Remote sensing and precision agriculture technologies for crop disease detection and management with a practical application example. *Engineering* 6, 528–532. <https://doi.org/10.1016/j.eng.2019.10.015>.
- Yang, C., 2012. A high-resolution airborne four-camera imaging system for agricultural remote sensing. *Comput. Electron. Agric.* 88, 13–24. <https://doi.org/10.1016/j.compag.2012.07.003>.
- Zaoui, S., Belmadani, A., 2021. Solving engineering optimization problems without penalty. *Int. J. Comput. Methods* 2150007. <https://doi.org/10.1142/S0219876221500079>.
- Zhang, J., Huang, Y., Pu, R., Gonzalez-Moreno, P., Yuan, L., Wu, K., Huang, W., 2019. Monitoring plant diseases and pests through remote sensing technology: A review in Computers and Electronics in Agriculture. 165, 104943. <https://doi.org/10.1016/j.compag.2019.104943>.
- Zhen, Z., Quackenbush, L.J., Zhang, L., 2016. Trends in automatic individual tree crown detection and delineation-evolution of LiDAR data. *Remote Sens.* 8. <https://doi.org/10.3390/rs8040333>.